The Oxidation Of Two Fe-Ce Alloys Under Low Oxygen Pressures at 600-800°C

by Y. Niu°, G.Y. Fu°@, W.T. Wu° and F. Gesmundo*

° *State Key Laboratory for Corrosion and Protection, Institute of Corrosion and Protection of Metals, CAS, Wencui Road 62, 110015 Shenyang (China).*

@ *Shenyang Institute of Chemical Technology, Aigongnan Street 11, 110021 Shenyang (China).*

* *Istituto di Chimica, Facolta' di Ingegneria, Universita' di Genova, Fiera del Mare, Pad. D, 16129 Genova (Italy).*

(Received February 19, 1998; final form April 15, 1998)

ABSTRACT

The corrosion of pure cerium and of two iron-based alloys containing approximately 15 and 30 wt% cerium was studied at 600-800°C in H_2-CO_2 mixtures providing at equilibrium oxygen pressure of 10^{-24} atm at 600°C and 10^{-20} atm at 700 and 800°C. The corrosion of the two alloys produced an internal attack, which transformed the cerium-rich phases into mixtures of iron metal and cerium-rich oxides, including a double Fe-Ce oxide as well as CeO_2. The rate of internal oxidation was much faster than expected on the basis of the solubility/diffusivity of oxygen in iron, especially for Fe-30Ce, for which oxygen penetration probably occurs mainly through microcracks produced by the large mechanical stresses associated with the local volume increase. The microstructures of the regions of internal oxidation followed closely those of the original alloys, while no cerium depletion was observed in the metal substrate. At 600 and 700°C some iron oxide formed on the alloy surface, while at 800°C a thin layer of pure iron metal formed on the surface of Fe-30Ce. These results are examined by taking into account the low solubility of cerium in iron and the presence of intermetallic compounds in the two alloys.

Key Words: iron, cerium, alloys, oxidation, internal attack

INTRODUCTION

The corrosion of binary Fe-Ce alloys, as well as of any alloy containing important amounts of cerium, has never been studied so far. On the other hand, the effect of the addition of small amounts of cerium on the high-temperature oxidation of alloys has been examined frequently. This is because one of the so-called reactive elements, when added at low levels (below 1wt%), can improve the oxidation resistance of ternary or more complex alloys forming protective external scales of chromia or alumina /1,2/. The corrosion of the present alloys has also been studied in H_2-H_2S mixtures at 600-800°C to establish whether the addition of significant contents of cerium could help to improve the poor sulfidation resistance of iron /3/. The same alloys are also being tested in atmospheres of low oxygen and relatively high sulfur pressures (around 10^{-20} atm O_2 and 10^{-8} atm S_2) /4/ which simulate the composition of atmospheres of industrial importance such as those involved in coal gasification /5,6/. The present study of their scaling behavior in purely oxidizing atmospheres of low oxygen activity has been undertaken to improve the understanding of the more complex behavior in mixed atmospheres, and also as a further example of corrosion of binary two-phase alloys, which may be used to check the correctness of the general predictions made in some recent theoretical papers /7-13/. The

behavior of pure cerium under the same conditions has also been examined for comparison purposes.

EXPERIMENTAL

Fe-Ce alloys with nominal cerium contents of 15 and 30 wt% (Fe-15Ce and Fe-30Ce, respectively) have been prepared by arc-melting mixtures of appropriate amounts of the two pure metals (99.99%) under Ti-gettered argon atmosphere. According to the Fe-Ce phase diagram /14/ (Fig. 1), the two alloys should be two-phase: more precisely, Fe-15Ce should be a mixture of pure iron (α phase) and the intermetallic compound $Fe_{17}Ce_2$ (β phase), while Fe-30Ce should contain a mixture of the β phase with Fe_2Ce (γ phase). For both alloys the actual microstructure (Fig. 2) is more complex than expected because they are composed of mixtures out of equilibrium of all the three phases α, β and γ, probably as a result of a slow peritectic reaction during cooling. Thus, the main difference between the two alloys is that for Fe-30Ce the volume fraction of the original α phase is smaller and those of the β and γ phases are larger than for Fe-15Ce. In addition, the average composition of the two alloys is not uniform, as commonly observed in two-phase binary systems, due to the absence of driving forces for diffusion in two-phase binary systems. However, the composition of Fe-30Ce is more uniform than that of Fe-15Ce.

Irregular samples with a surface area of about 2.5 cm^2 were obtained by cutting the original ingots by means of a diamond-wheel saw. They were ground down to 600 grit emery paper, washed in water, alcohol and acetone and dried immediately before use. Corroded samples were examined by means of X-ray diffraction (XRD), optical microscopy (OM) and electron scanning microscopy (SEM) for phase identification and structural analysis.

Kinetics measurements were carried out by means of a Cahn microbalance mod. 2000. The corrosive gases were composed of H_2-CO_2 mixtures of appropriate composition, providing 10^{-24} atm O_2 at 600°C and 10^{-20} atm O_2 at 700 and 800°C. These mixtures were obtained from cylinders of premixed H_2-CO_2 gases containing 61.0, 79.4 and 13.2 vol.% CO_2 at 600, 700 and 800°C, respectively.

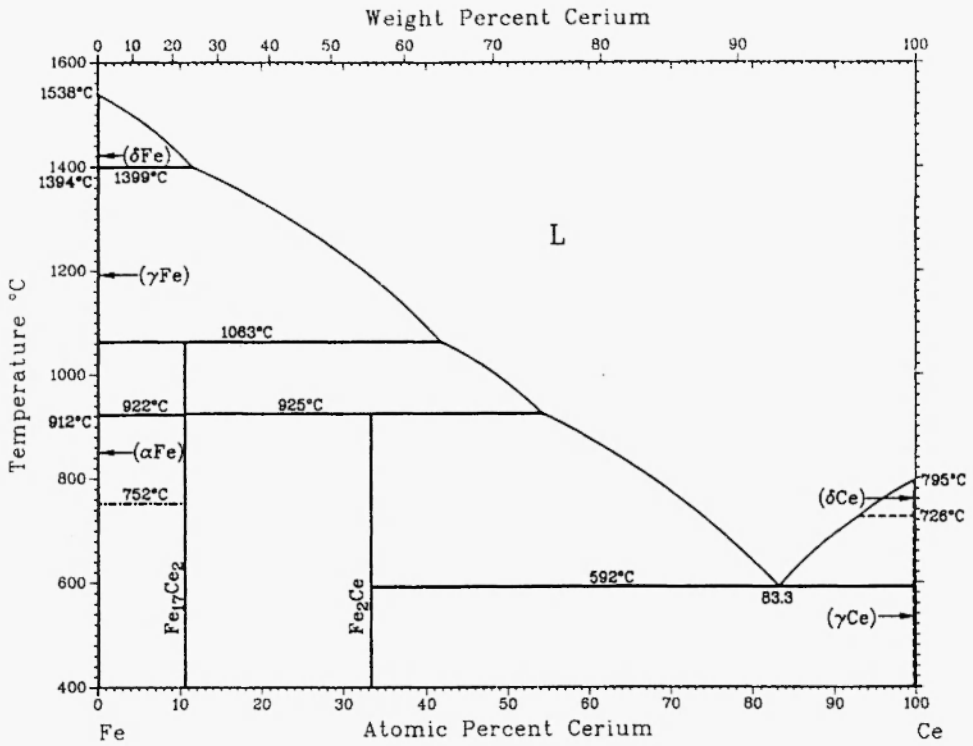

Fig. 1: Phase diagram of the binary system Fe-Ce (from Ref. [14]).

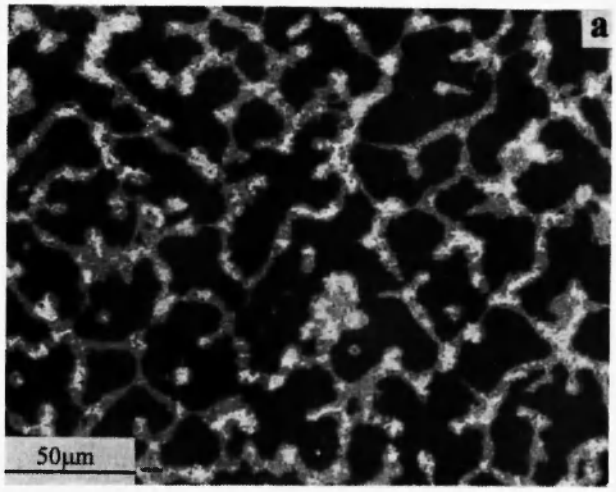

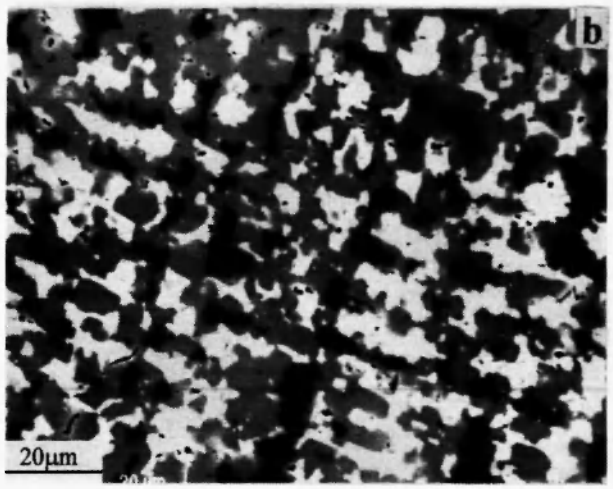

Fig. 2: Microstructures of the Fe-15Ce (Fig. 2a) and Fe-30Ce (Fig. 2b) alloys. dark phase: α-Fe; medium gray phase: β-$Fe_{17}Ce_2$; light phase: γ-Fe_2Ce.

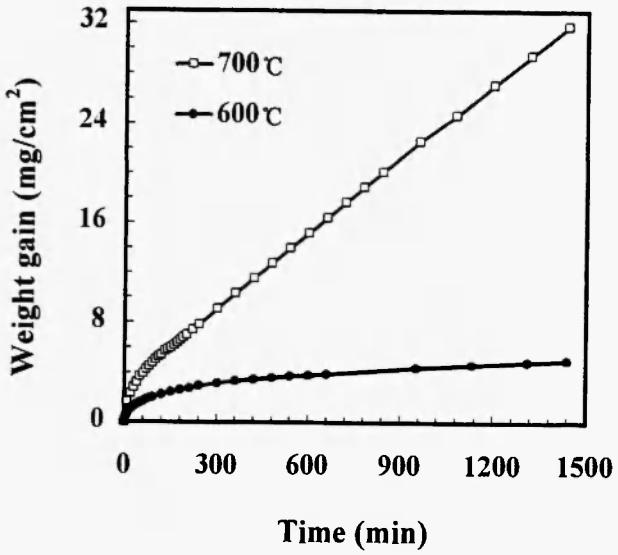

Fig. 3: Oxidation kinetics of pure cerium in H_2-CO_2 mixtures under 10^{-24} atm O_2 at 600°C and 10^{-20} atm O_2 at 700°C.

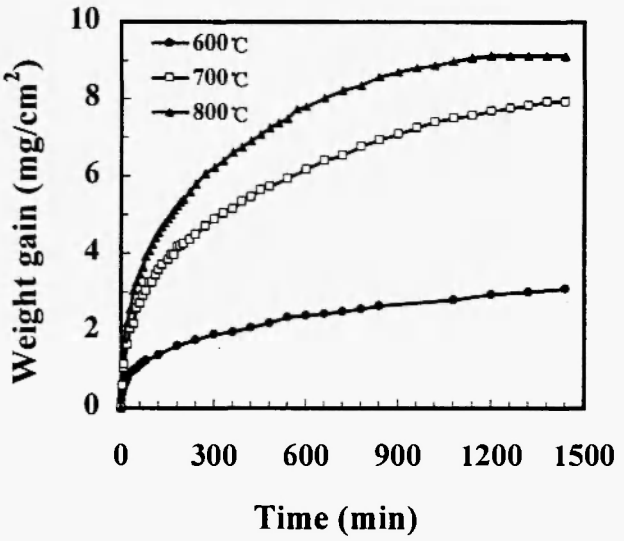

Fig. 4: Oxidation kinetics of Fe-15Ce in H_2-CO_2 mixtures under 10^{-24} atm O_2 at 600°C and 10^{-20} atm O_2 at 700°C and 800°C.

RESULTS

A - Kinetics

Kinetics plots for pure cerium and the two alloys are shown separately in Figs. 3-5, respectively. The oxidation of pure cerium (Fig. 3) was studied only at 600 and 700°C because the pure metal melts below 800°C. At 600°C the oxidation rate of pure cerium decreases with time but the instantaneous parabolic rate constant (iprc), i.e. the slope of the square of the weight gain vs time, increases with time, so that the kinetics are intermediate between linear and parabolic. At 700°C an initial quasi-parabolic stage of about 6 hr is followed by an approximately linear stage.

At all temperatures the oxidation rate of Fe-15Ce (Fig. 4) decreased continuously with time more rapidly than according to the parabolic rate law, so that the iprc is also decreasing continuously with time. In particular,

samples of Fe-15Ce corroded at 800°C were completely reacted before the end of the test (24 hr).

The corrosion of Fe-30Ce (Fig. 5) was very rapid and was almost completed after quite a short time (Fig. 5a). Moreover, the oxidation rate during the initial stage increased with temperature (Fig. 5b). At 600°C Fe-30Ce showed an initial parabolic period of about 5 hr, after

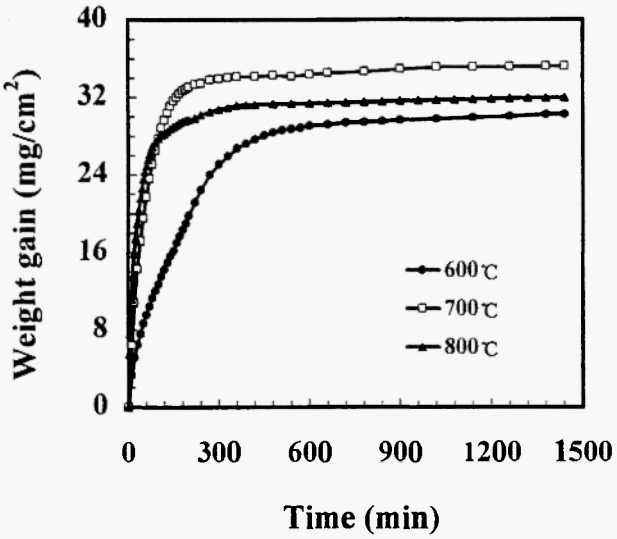

a

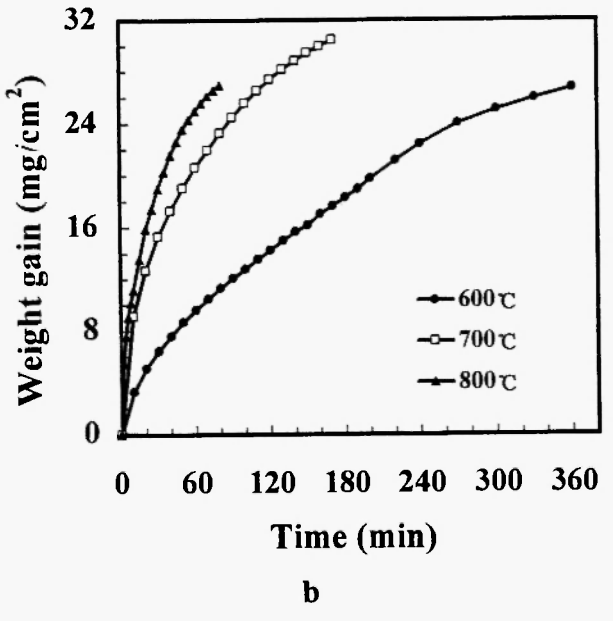

b

Fig. 5: Kinetics of Fe-30Ce in H_2-CO_2 mixtures under 10^{-24} atm O_2 at 600°C and 10^{-20} atm O_2 at 700-800°C.
Fig. 5a: 24 hr results;
Fig. 5b: short-term results.

which the rate first increased slightly and then decreased rapidly to become very small and approximately constant after about 10 hr. At 700°C during an initial stage of about 3 hr the rate decreased, but the iprc increased, indicating kinetics intermediate between linear and parabolic: after this, the rate decreased rapidly, becoming very low and nearly equal to zero after about 6 hr. At 800°C both the rate and the iprc decreased with time from the start of the test, while the weight became constant after about 2 hr. The differences between the overall weight gains measured after a long time (24 hr), which correspond to a complete oxidation of the samples, do not have any special meaning, because they depend on the thickness of the samples, which was not the same for all the tests. Short-term tests were carried out for this alloy at 700 and 800°C for microstructural investigations. Approximate values of the parabolic rate constants for the two alloys and pure cerium, calculated when possible from the appropriate sections of the kinetics curves, are given in Table I.

B - Scale microstructure and composition

Micrographs of cross-sections of Fe-15Ce corroded at 600, 700 and 800°C are shown in Figs. 6, 7 and 8, while the corresponding micrographs for Fe-30Ce are shown in Figs. 9, 10 and 11, respectively. For these samples the depth of the region of internal oxidation can be seen in the micrographs only through a slight change in color, because, due to the presence of oxygen, the zone of internal oxidation appears darker than the alloy. On the contrary, the microstructures of the region of internal oxidation and of the original alloy are very similar to each other, even though the real situation of the oxidized sample layers is more complex. In fact, while the α phase does not undergo any chemical change as a consequence of the presence of oxygen, the cerium-containing phases are transformed into a mixture of iron metal and the cerium oxide CeO_2 as well as some double Fe-Ce oxide $FeCe_2O_4$. However, the mixtures of phases produced by the solid-state reaction of the cerium-rich phases with oxygen are composed of very small particles which in most cases cannot be resolved, while the internal oxidation does not involve any important diffusion of cerium. Therefore, the

Table 1

Approximate parabolic rate constants ($g^2\ cm^{-4}\ s^{-1}$) for pure cerium and the two Fe-Ce alloys corroded in H_2-CO_2 mixtures under 10^{-24} atm O_2 at 600°C and 10^{-20} atm O_2 at 700-800°C

T (°C)		600°C	700°C	800°C
Fe-15Ce	(i)	4.8×10^{-10}	2.2×10^{-9}	3.0×10^{-9}
	(av)	1.0×10^{-10}	4.6×10^{-10}	7.5×10^{-10}
	(f)	4.6×10^{-11}	2.6×10^{-10}	8.4×10^{-11}
Fe-30Ce	(i)	3.8×10^{-8}	1.3×10^{-7}	1.7×10^{-7}
	(av)	-	-	-
	(f)	-	-	-
Ce	(i)	9.2×10^{-10}	4.2×10^{-9}	-
	(av)	1.4×10^{-10}	-	-
	(f)	2.8×10^{-10}	linear	-

i = initial values, av = average values; f = final values

microstructure of the zone of internal oxidation is strictly related to that of the original alloy. Moreover, the internal oxidation does not involve any depletion of cerium in the alloy ahead of the internal oxidation front, as evidenced by the absence of formation of an α layer at this site. The presence of some Fe_3O_4 in the samples corroded at 600 and 700°C, when the oxygen pressure in the gas was above the dissociation pressure of the iron oxides, was only detected by means of XRD but not by SEM, so that only small amounts of iron oxides must have formed.

Oxidation of Fe-15Ce at 600 and 700°C for 24 hr (Figs. 6 and 7, respectively) produces a thick layer of internal oxidation (about 250 microns at 600°C and 500 microns at 700°C), containing a mixture of α iron, the double oxide $FeCe_2O_4$ and CeO_2, as revealed by XRD. However, in the inner section of the region of internal oxidation other cerium oxides stable at lower oxygen pressures, such as Ce_2O_3 and/or CeO, can also form. The dark islands in Fig. 7b correspond to iron metal (α phase): their size, number, shape and spatial distribution correspond closely to those of the particles of the α phase in the original alloy. On the contrary, the islands of β phase transform into a mixture of iron metal with cerium-rich compounds which generally looks uniform (gray zones). The size of the individual phase particles inside these islands is too small for EDX analysis. The average composition of these gray zones corresponds to iron/cerium atomic ratios equal to those typical of the β phase. Finally, the particles of γ phase upon oxidation form light regions containing again a mixture of α iron and Ce-rich compounds, while the average composition in terms of the two metals is the same as that of the metallic γ phase before oxidation. After oxidation at 700°C at some places the outermost layer of internal oxidation appears different from the zone deeper into the alloy (Fig. 8c). A similar effect was observed in the past for the internal oxidation of Fe-Nb alloys under the same conditions and was due to the formation of double Fe-Nb oxides close to the alloy surface /15/. The

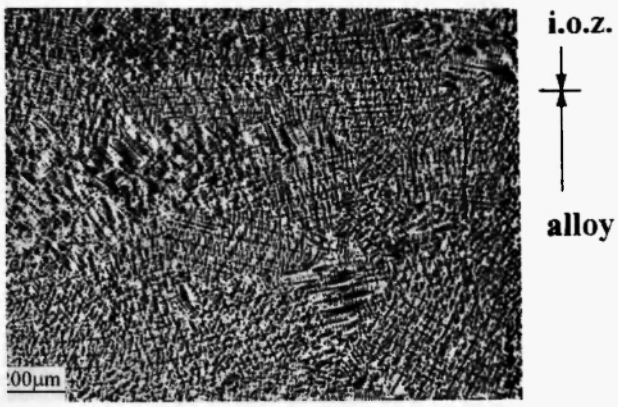

Fig. 6: Micrograph of a cross section of Fe-15Ce oxidized for 24 hr in a H_2-CO_2 mixture under 10^{-24} atm O_2 at 600°C (SEM/BEI).

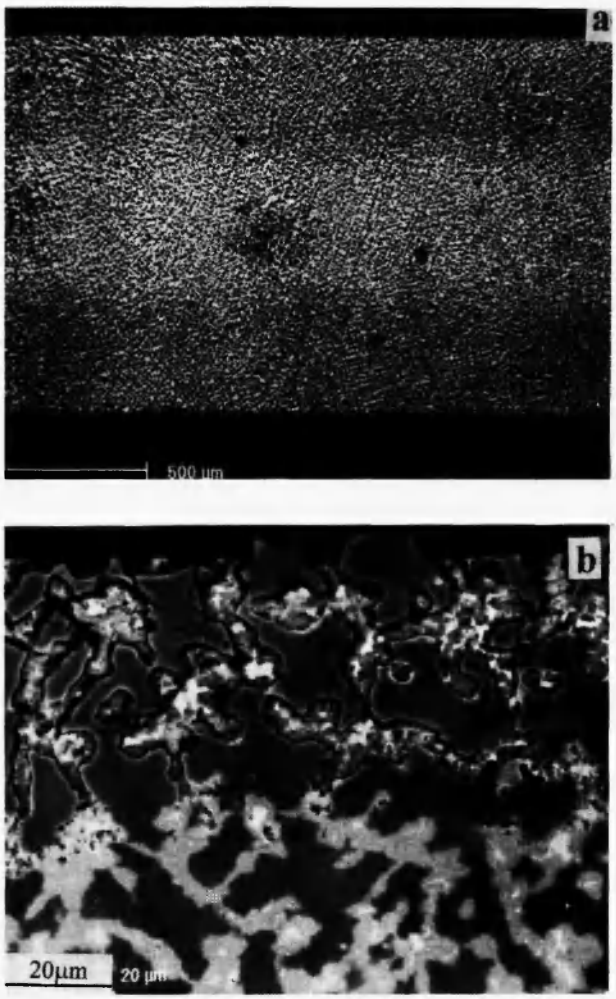

Fig. 7: Micrographs of cross sections of Fe-15Ce oxidized for 24 hr in a H_2-CO_2 mixture under 10^{-20} atm O_2 at 700°C (SEM/BEI).
Fig. 7a: general view;
Fig. 7b: expanded view of the alloy/gas interface.

changes observed for the present sample are probably due to the same reason. In view of the fact that for thermodynamic reasons the double oxides are only stable in the external section of the internal oxidation zone /16/, it is concluded that the Ce-rich compounds formed by internal oxidation are the two double Fe-Ce oxides in the external part of this zone and CeO_2 deeper into the alloy.

A sample of Fe-15Ce exposed at 800°C for 24 hr, but not completely corroded due to a larger thickness than the sample whose weight-gain curve is shown in

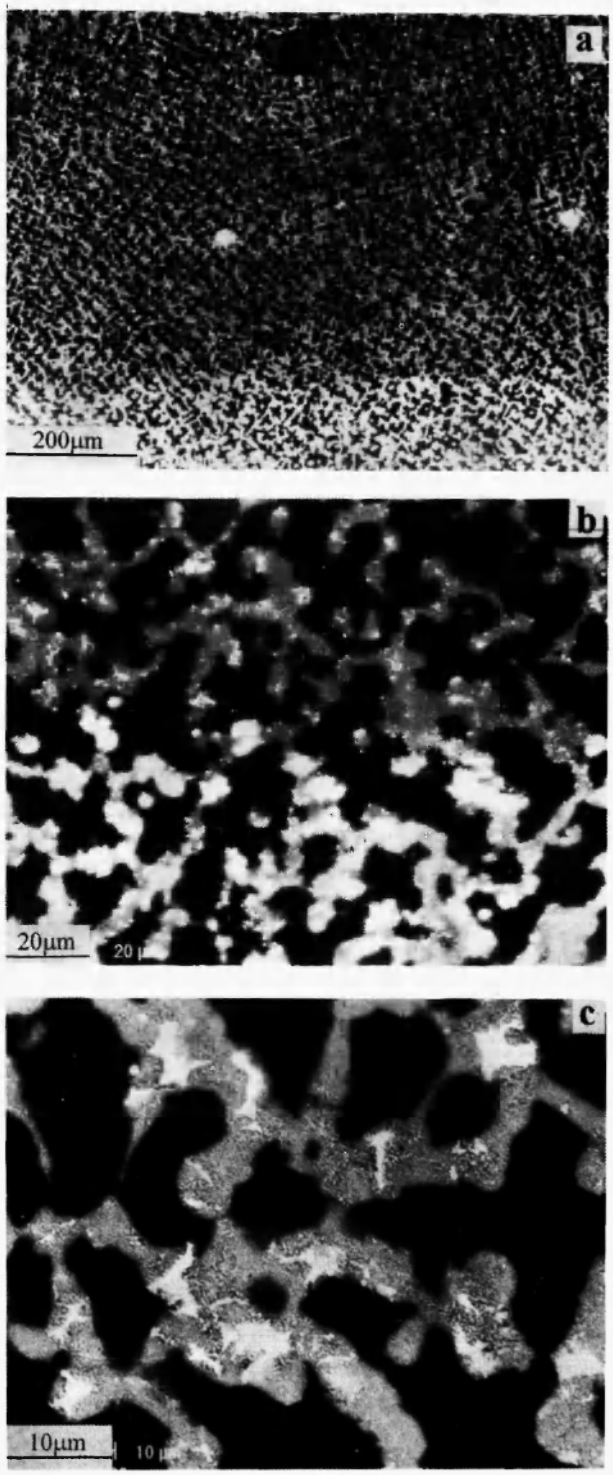

Fig. 8: Micrographs of cross sections of Fe-15Ce oxidized for 24 hr in a H_2-CO_2 mixture under 10^{-20} atm O_2 at 800°C.
Fig. 8a: general view (SEM/SEI);
Fig. 8b: expanded view of the internal oxidation front (SEM/SEI); Fig. 8c: expanded view of the internal oxidation zone (SEM/BEI).

the kinetics plot (Fig. 8a), shows a region of internal oxidation about 520 microns thick with the same microstructure as that observed at lower temperatures. An enlarged view of the internal oxidation front (Fig. 8b) shows clearly the difference between the alloy and the region of internal oxidation as well as the similarity of the microstructure between the two zones. The internal oxidation zone involves always the presence of three different regions corresponding to the three phases in the original alloy (Fig. 8c): in particular, the light and gray regions are strongly intermixed, since the gray islands contain a continuous distribution of light particles of different size.

Samples of Fe-30Ce corroded at 600°C (Fig. 9), 700°C (Fig. 10) and 800°C (Fig. 11) for relatively short times to avoid complete reaction, and thus different from those used to generate the weight gains shown in the kinetics plots, show in all cases an outermost layer rather porous and generally cracked, followed by an inner compact layer. More precisely, the samples shown in Figs. 9, 10 and 11 have been corroded for 20 min, 20 min and 4 min, respectively, while the overall thickness of their internal oxidation region is of 250, 360 and 500 microns. In all cases the region of internal attack is actually divided into two layers, denoted as L_1 and L_2, divided by a rather sharp interface, I_1, while I_2 is the interface between the zone of internal oxidation and the alloy (Figs. 9a and 11a): at 700°C the difference between the two layers becomes not clear (Fig 10).

Enlarged views of the region across the interface I_2 (Figs. 9c and 11c) show that in moving from the alloy into the region of internal oxidation the appearance of the α and β islands does not change, while the islands of γ phase become darker than in the alloy and rather porous. Enlarged views of the region across the interface I_1 (Figs. 9b and 11b) show that the α phase still remains unchanged, while the β phase in the layer L_1 becomes darker than in the layer L_2. Finally, the γ phase islands become lighter in the layer L_1 than in the layer L_2 and are not uniform in color, being actually composed of a light gray matrix which contains some whiter particles. In some cases these white particles are large enough to be examined by EDX and result to be composed of pure cerium oxide. It seems likely that the light matrix is composed of a mixture of iron with CeO_2, but with a larger content of CeO_2 than the

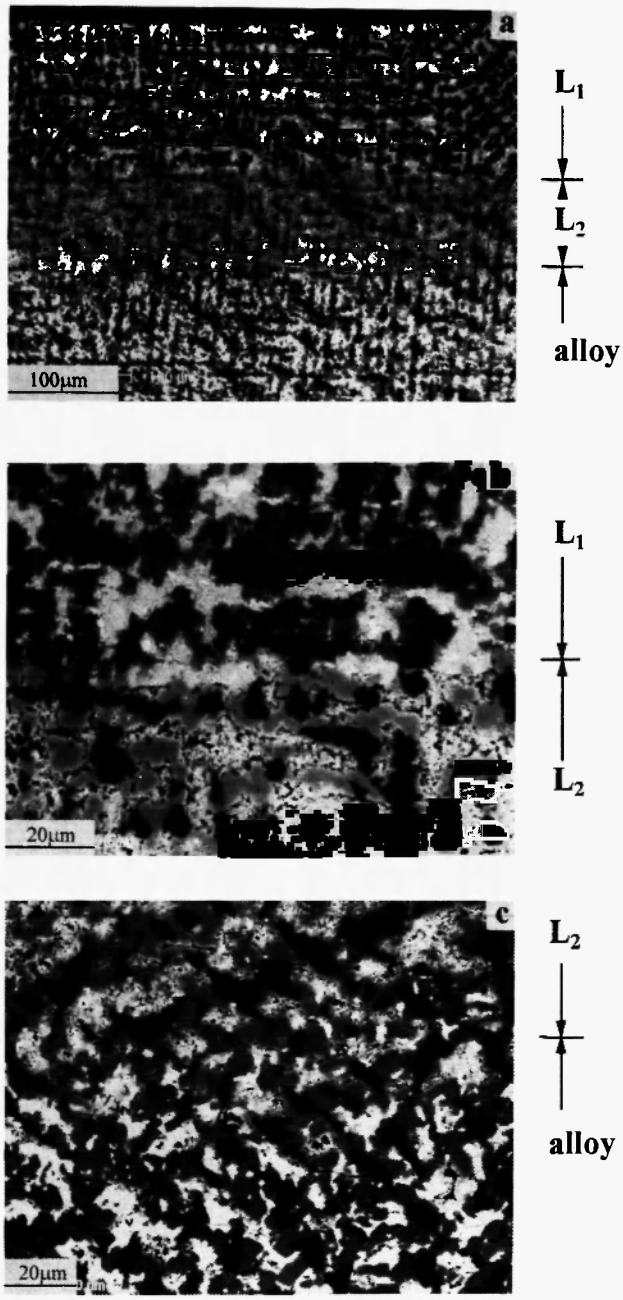

Fig. 9: Micrographs of cross sections of Fe-30Ce oxidized for 20 min in a H_2-CO_2 mixture under 10^{-24} atm O_2 at 600°C (SEM/BEI).
Fig. 9a: general view;
Fig. 9b: expanded view of the interface between the outer (L_1) and inner (L_2) layers of internal oxidation;
Fig. 9c: expanded view of the interface between the alloy and the inner layer (L_2) of internal oxidation.

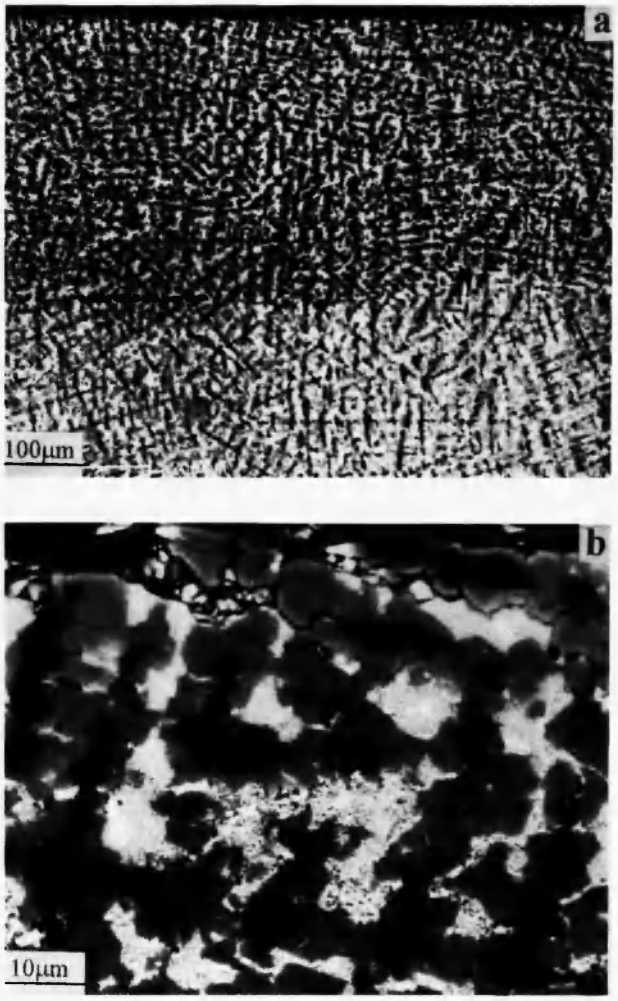

Fig. 10: Micrographs of cross sections of Fe-30Ce oxidized for 20 min in a H_2-CO_2 mixture under 10^{-20} atm O_2 at 700°C (SEM/BEI).
Fig. 10a: general view;
Fig. 10b: expanded view of the alloy/gas interface.

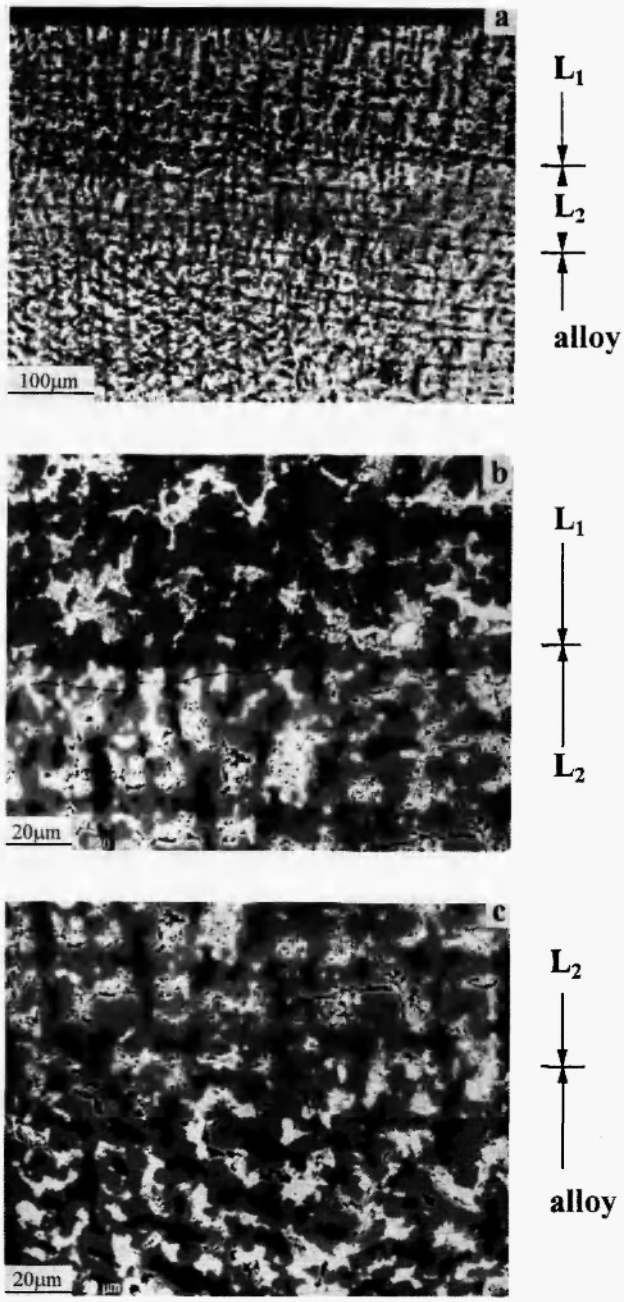

Fig. 11: Micrographs of cross sections of Fe-30Ce oxidized for 4 min in a H_2-CO_2 mixture under 10^{-20} atm O_2 at 800°C (SEM/BEI).
Fig. 11a: general view;
Fig. 11b: expanded view of the interface between the outer (L_1) and inner (L_2) layers of internal oxidation;
Fig. 11c: expanded view of the interface between the alloy and the inner layer (L_2) of internal oxidation.

middle-gray regions formed by oxidation of the β phase. The exact reasons for the difference between the layers L_1 and L_2 are not clear, but they should be connected with a smaller oxygen content than in layer L_1. It seems possible that the layer L_2 may contain a cerium oxide lower than CeO_2. At 700 and 800°C a relatively thin layer of the outermost region of internal oxidation region (about 0.1 of the overall thickness of the internal oxidation region at 700°C and 0.3 at 800°C) (Figs. 10b and 11a) is different from the layer L_1 for what concerns

the appearance of the regions produced by oxidation of the γ islands, inside which the white CeO_2 particles disappeared almost completely. It seems very likely that this change is due to the reaction of CeO_2 with iron and oxygen to form the double oxide, as already noted above. Finally, samples of Fe-30Ce corroded at 800°C show also an outermost thin layer of pure iron metal.

DISCUSSION

The superimposed phase diagrams of the binary Fe-O and Ce-O systems are shown in Fig. 12 with an indication of the partial pressures of oxygen used in this work. At 600 and 700°C the oxygen pressure in the gas is in the field of stability of Fe_3O_4, while at 800°C it is in that of iron metal. Thus, at 600 and 700°C the alloys should form an external layer of iron oxide, which however is not observed, at variance with the results for the corresponding Fe-Y alloys /17/. On the contrary, the oxygen pressures used are always much higher than for the cerium-cerium oxide equilibrium, so that this element should be oxidized either internally or externally to the alloys. The formation of double Fe-Ce oxides is also possible because the partial oxygen pressures required for their formation are lower than for the oxidation of pure iron. Although the thermodynamic

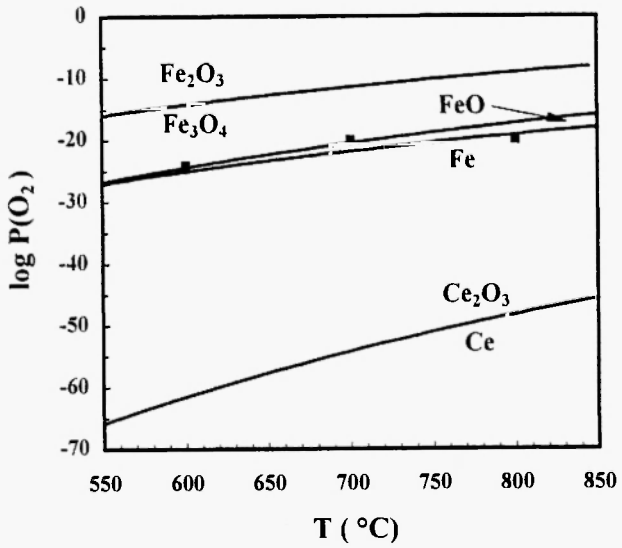

Fig. 12: Superimposed phase diagrams of the binary Fe-O and Ce-O systems with an indication of the oxygen pressures used in this work.

stability of the double oxide $FeCe_2O_4$ (d.o.) is not known, it may be estimated by recalling that the standard free energy change associated with a combination of two pure oxides to form a double oxide, such as

$$FeO + Ce_2O_3 = FeCe_2O_4 \quad (r)$$

ranges generally between –20 and –40 kJ/mol /18/. Thus, taking $\Delta G°(r) = -40$ kJ/mol, using the known stabilities of FeO and Ce_2O_3, a solubility of 0.082 wt% and an activity coefficient of 10^{-3} for cerium in iron, it is possible to calculate a pressure of 1.04×10^{-19} atm O_2 for the Fe-FeO-d.o. equilibrium and of 1.15×10^{-23} atm O_2 for the Fe-d.o.-Ce_2O_3 equilibrium at 800°C, the second of which is significantly lower than that used in the gas at this temperature.

A schematic form of the isothermal phase diagram for the ternary Fe-O-Ce system involving only the oxides FeO and Ce_2O_3, the double oxide $FeCe_2O_4$ and the four metal phases is shown in Fig. 13. In view of the large difference between the stabilities of the iron and cerium oxides, the alloy composition for the simultaneous equilibrium with the two oxides is assumed to fall in the field of existence of the α phase, in spite of the small solubility of cerium in iron (0.088 wt% Ce at 850°C /14/). The partial pressures of oxygen for the various equilibria are denoted as P_1 (α-FeO- d.o.), P_2 (pure Fe-FeO), P_3 (α-d.o.-Ce_2O_3), P_4 (α-β-Ce_2O_3), P_5 (β-γ-Ce_2O_3), P_6 (γ-δ-Ce_2O_3) and P_7 (pure Ce-Ce_2O_3), while the value prevailing in the gas phase is denoted P^g. Since the oxygen pressure in the gas is below the value for the Fe/FeO equilibrium, the diagram corresponds to the situation of the present study at 800°C. However, the situation at the lower temperatures will only be slightly different, involving only the additional possibility of formation of an outermost layer of pure iron oxide. Moreover, the oxygen pressure P_3 must be lower than P^g because otherwise the double oxide would not have formed under the present conditions at 800°C.

The diffusion path corresponding to the structure of the internal oxidation region observed for these samples corresponds simply to a vertical straight line, implying a substantial absence of an important diffusion of cerium in the alloy /9,11/. This type of internal attack, denoted

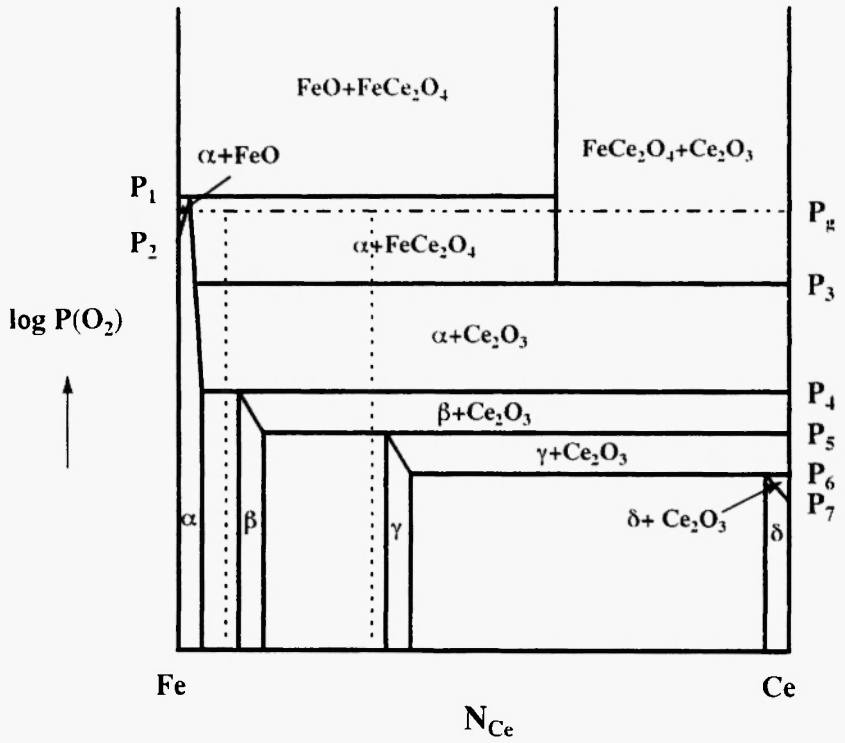

Fig. 13: Schematic isothermal phase diagram of the ternary Fe-Ce-O system with an indication of the actual diffusion paths (dashed lines).

as in-situ or diffusionless internal oxidation, has been predicted to occur in the oxidation of binary alloys presenting a small solubility of the two components /9,11-13/. Under these conditions, the kinetics of internal oxidation are entirely controlled by the rate of inward penetration of oxygen in the alloy /12,13/.

The internal oxidation of the present alloys is very fast, especially for Fe-30Ce, whose samples about 1 mm thick were completely corroded within 1-10 hr, depending on temperature. The kinetics of internal oxidation of these alloys may be calculated as a first approximation by neglecting the outward diffusion of cerium and the hindering effect on the rate of oxygen penetration due to the presence of large volume fractions of internal oxide. If the internal oxidation of the component B of binary A-B alloys by a single oxidant follows the parabolic rate law, the depth of i.o., ξ, changes with time according to the equation /19,20/

$$\xi^2 = 4\,\gamma^2\,D_O\,t \qquad (1)$$

where D_O is the diffusion coefficient of oxygen in the base metal and t is time. For solid-solution alloys the kinetics parameter γ in Eq.(1) may be calculated from the equation

$$N_O^s/\nu\,N_B^\circ = G(\gamma)/F(h) \qquad (2a)$$

given by Wagner /19/, where N_B° is the bulk content of B (mole fraction), ν the oxygen/B ratio in BO_ν and $h = \gamma\,\varphi^{1/2}$, while φ is equal to D_O/D_B, where D_B is the diffusion coefficient of B in the alloy and G(r) and F(r) are the two auxiliary functions

$$G(r) = \pi^{1/2}\,r\,\exp(r^2)\,\mathrm{erf}(r)$$

and

$$F(r) = \pi^{1/2}\,r\,\exp(r^2)\,\mathrm{erfc}(r)\,.$$

For two-phase alloys in the absence of important outward diffusion of the reactive component the previous equation takes the form /21/

$$N_O^s/\nu\,N_B^{av} = G(\gamma) \qquad (2b)$$

where N_B^{av} is the average content of B in the alloy. Finally, if the effect of the presence of a volume fraction, f_v, of internal oxide on the inward diffusion of oxygen is taken into account, Eq. (2b) becomes /21/

$$N_O^S (1-f_v)/v \; N_B^{\xi v} = G(\gamma) \qquad (2c)$$

The parameter f_v is given by

$$f_v = N_{ox}/[R - N_{ox}(R-1)]$$

where R is the ratio between the molar volumes of the alloy and the internal oxide and N_{ox} the mole fraction of internal oxide, which in turn is given by

$$N_{ox} = 1 - [1 - N_B^{av}]/[1 - N_B^{s}(\alpha)]$$

where $N_B^{s}(\alpha)$ is the solubility of B in the α phase.

The solubility of oxygen in α iron at the pressure for the Fe/FeO equilibrium is given by /22/

$$N_O^{so} = 0.381 \exp(-104 \text{ kJ/mol/RT})$$

while the diffusivity of oxygen in iron is given by /22/

$$D_O (cm^2 s^{-1}) = 1.79 \times 10^{-3} \exp(-85.7 \text{ kJ/mol/RT})$$

Using Sievert's law to calculate N_O^s under the gas-phase oxygen pressure and assuming for simplicity the formation of CeO_2 only, Eqs.(2b) and (2c) allow calculation of the depths of internal oxidation reported in Table II, which are much smaller than those measured experimentally and reported earlier. Thus, oxygen penetrates in the alloys much more rapidly than by normal bulk diffusion. A similar situation was already found in the oxidation of M-Nb alloys (with M = Fe, Co and Ni) under the same oxygen pressures and the same temperatures used here /21/ as well as in the oxidation of Ni-Al alloys /23/. The large increase in the rate of internal oxidation has been explained by assuming that oxygen may diffuse inwards through the base-metal matrix both along the metal-oxide interface and along short-circuit paths such as dislocation lines produced by the large stresses associated with the increase in volume due to internal oxidation /21,23/. The experimental values of the depth of internal oxidation can be obtained using again Eqs.(2b) or (2c), but multiplying the diffusion coefficient of oxygen in iron by suitable enhancement factors /21/, which are reported in Table III for the various cases. These factors, which are already quite large for Fe-15Ce, become extremely large for Fe-30Ce, for which the observed effect must have another origin. For this alloy it is proposed that the stresses induced by the internal oxidation of cerium may produce microcracks through which oxygen can penetrate extremely rapidly, as observed.

Table 2

Experimental and calculated values (μm) of the internal oxidation depths (i.o.d.) for the two Fe-Ce alloys after the given oxidation times

T (°C)		600	700	800
	time (hr)	24	24	24
Fe-15Ce	i.o.d. (exper.)	250	500	520
	i.o.d. (cal.-A)	0.7	2.8	5.0
	i.o.d. (cal.-B)	0.6	2.6	4.6
	time (min.)	20	20	4
Fe-30Ce	i.o.d. (exper.)	250	360	500
	i.o.d. (cal.-A)	0.05	0.22	0.18
	i.o.d. (cal.-B)	0.04	0.18	0.15

A - calculated by means of Eq.(2b), B - calculated by means of Eq.(2c)

Table 3

Enhancement factors (e.f.) for the oxygen diffusion coefficient to produce the depths of internal oxidation measured experimentally

T (°C)		600	700	800
	time (hr)	24	24	24
Fe-15Ce	e.f. - A	1.3×10^5	3.1×10^4	1.1×10^4
	e.f. - B	1.6×10^5	3.7×10^4	1.3×10^4
	time (min.)	20	20	4
Fe-30Ce	e.f. - A	2.1×10^7	2.6×10^6	8.0×10^6
	e.f. - B	3.1×10^7	3.8×10^6	1.2×10^7

A - calculated by means of Eq.(2b), B - calculated by means of Eq.(2c)

An important consequence of the *in-situ* type of internal oxidation of two-phase alloys is that the microstructure of the corrosion-affected region is closely related to that of the original alloy, as reported above. In particular, if the alloy contains a mixture of the solid solution of B in A (α phase) and of the next phase richer in B in the A-B phase diagram (β phase), as the present Fe-15Ce alloy, the α phase will remain in the metal state, while the β phase will transform into a very fine mixture of A and BO. Moreover, the spatial distribution of the BO particles formed by oxidation of the β phase will correspond closely to that of the β islands phase in the original alloy. The behavior of the present alloys is in agreement with this prediction, even though the actual microstructures of the regions of internal oxidation are significantly more complex due to the simultaneous presence of three phases and to the existence of large amounts of iron also in the Ce-containing phases.

These alloys were never observed to form an external layer of cerium oxide, even though the cerium content of Fe-30Ce is rather high (about 15 at %). The main reason for this is probably the very low solubility and possible low diffusivity of cerium in the α phase, with the consequent presence of intermetallic Fe-Ce compounds. In addition, the stability ranges of these compounds are quite restricted, so that diffusion of cerium should be slow even through them This is in agreement with the conclusions of a general paper concerning the internal oxidation of the most-stable component B of two-phase binary A-B alloys and the transition to the formation of external BO scales /12,13/. In fact, the critical concentration of B required for this transition is higher for two-phase than for solid-solution alloys and increases as the solubility of B in A decreases /12,13/.

The effect of the presence of variable amounts of the double oxide $FeCe_2O_4$ in the outer region of the scales on the overall scaling kinetics of these alloys cannot be discussed in any detail, because its transport properties are totally unknown. Moreover, the rates of matter transport through multiphase layers such as those observed here depend not only on the properties of the single phases as well as on their respective volume fractions and spatial distribution, but may also involve significant contributions from the diffusion along grain boundaries, especially those between different phases, so that they are practically impossible to predict.

Finally, a layer of pure iron metal free from oxide inclusions formed on the sample surface at 800°C. An outward diffusion of the base metal during the internal oxidation of binary alloys, which however produced essentially isolated nodules of metal at the external alloy surface rather than continuous layers, has already been reported in some cases /24-27/. The formation of a continuous external layer of the solvent metal has also

been observed in the oxidation of a Co-15wt% yttrium /28/ and of a Co-15 wt% cerium /29/ alloy under the same conditions as used in this work. This outward diffusion of the solvent metal has been attributed by Guruswami *et al.* /24/ to the existence of large mechanical stresses produced by the increase in volume associated with the internal oxidation. The process observed here has very likely the same origin and is a further proof of the accumulation of large stresses due to the internal oxidation of cerium in these samples.

CONCLUSIONS

The oxidation of two Fe-Ce alloys under low oxygen pressures at 600-800°C produces an internal oxidation of cerium much faster than expected on the basis of the solubility/diffusivity of oxygen in iron, especially at high temperatures and high cerium contents. Iron forms small amounts of oxides at 600 and 700°C, when the oxygen pressure in the gas is in the field of stability of Fe_3O_4, and a thin outermost layer of pure metal at 800°C (only on Fe-30Ce), when the oxygen pressure in the gas is in the field of stability of iron. The formation of external scales of CeO_2 is never observed. Other important aspects of the oxidation of these alloys are the absence of any depletion of cerium in the alloy and the close relation between the microstructure of the corrosion-affected regions and that of the original alloys. In fact, upon oxidation the islands of α phase remain unchanged while those of β and γ phase are converted into complex mixtures of α iron, cerium oxide and/or double iron-cerium oxide without involving any significant diffusion of cerium. All these properties are a direct consequence of the low solubility of cerium in the base metal and of the presence of one or two intermetallic compounds in the alloy.

ACKNOWLEDGMENTS

Financial support for this work, partially by the European Community through the Research Contract N. CTI1*-CT94-0007 and partially by the NNSF in China through a grant N. 59735101, is gratefully acknowledged.

REFERENCES

1. P. Kofstad, *High Temperature Corrosion*, Elsevier Applied Science, New York, 1988.
2. E. Lang, *The Role of Active Elements in the Oxidation Behaviour of High Temperature Alloys*, Elsevier Applied Science, New York, 1989.
3. Y. Niu, P. Castello, G.Y. Fu and F. Gesmundo, *Corros. Sci.*, **39**, 1845 (1997).
4. Y. Niu, G.Y. Fu and F. Gesmundo, to be published.
5. F. Gesmundo, D.J. Young and S.K. Roy, *High Temperature Materials and Processes*, **8**, 149 (1980).
6. J. Stringer, in *High-Temperature Oxidation and Sulfidation Processes*, J.D. Embury (ed.), Pergamon Press, New York, 1990; p. 257.
7. F. Gesmundo, Y. Niu, F. Viani and D.L. Douglass, *Oxid. Met.*, **39**, 197 (1993).
8. F. Gesmundo, Y. Niu, F. Viani and D.L. Douglass, *Oxid. Met.*, **40**, 373 (1993).
9. F. Gesmundo, F. Viani and Y. Niu, *Oxid. Met.*, **42**, 409 (1994).
10. F. Gesmundo, F. Viani, Y. Niu and D.L. Douglass, *Oxid. Met.*, **42**, 465 (1994).
11. F. Gesmundo, Y. Niu and F. Viani, *Oxid. Met.*, **43**, 379 (1995).
12. F. Gesmundo, F. Viani and Y. Niu, *Oxid. Met.*, **45**, 51 (1996).
13. F. Gesmundo, F. Viani and Y. Niu, *Oxid. Met.*, **47**, 355 (1997).
14. *Binary Alloys Phase Diagrams*, T.B. Massalski, J.L. Murry, L.H. Bennett and H. Baker (Eds.), ASM, Materials Park (1986).
15. M.C. Rebello, Y. Niu, F. Rizzo and F. Gesmundo, *Oxid. Met.*, **43**, 561 (1995).
16. J. Megusar and G.H. Meier, *Met. Trans.*, **7A**, 1133 (1976).
17. Y. Niu, R.Y. Yan, W.T. Wu, F. Gesmundo and G.Y. Fu, *Oxid. Met.*, 49, 91 (1997).
18. O. Kubaschewski, *High Temp.-High Press.*, **4**, 1 (1972)
19. C. Wagner, *Z. Elektrochem.*, **63**, 772 (1959).
20. R.A. Rapp, *Corrosion*, **21**, 382 (1965).
21. F. Gesmundo, Y. Niu, F.Viani and F.C. Rizzo, *Oxid. Met.*, **46**, 441 (1996).

22. J. Takada, S. Yamamoto, S. Kikuchi and M. Adacki, *Oxid. Met.*, **25**, 93 (1986).
23. F.H. Stott and G.C. Wood, *Mater. Sci. Technol.*, **4**, 1072 (1988).
24. S. Guruswami, S.M. Park, J.P. Hirth and R.A. Rapp, *Oxid. Met.*, **26**, 77 (1986).
25. D.L. Douglass, B. Zhu an F. Gesmundo, *Oxid. Met.*, **38**, 365 (1992).
26. R.P. Rubly and D.L. Douglass, in: *High-Temperature Corrosion of Advanced Materials and Protective Coatings*, Y. Saito and B. Onay (eds.), Elsevier, Amsterdam, 1992; p. 133.
27. D.L. Douglass, *Oxid. Met.*, **44**, 81 (1995).
28. W.T. Wu, R.Y. Yan, Y. Niu and F. Gesmundo, *Corros. Sci.*, **39**, 1831 (1997).
29. G.Y. Fu, Y. Niu, W.T. Wu and F. Gesmundo, *Corros. Sci.*, accepted for publication.